

Precise parameter determination of the open cluster NGC 1647 via asteroseismology of p -mode pulsators

MINGFENG QIN,^{1,2} JIAN-NING FU,^{1,2,3} WEIKAI ZONG,^{1,2} TIANQI CANG,^{1,2} ANTONIO FRASCA,⁴ GANG MENG,^{1,2} AND XIRAN XIE²

¹*Institute for Frontiers in Astronomy and Astrophysics, Beijing Normal University, Beijing 102206, P. R. China*

²*School of Physics and Astronomy, Beijing Normal University, Beijing 100875, P. R. China*

³*Xinjiang Astronomical Observatory, Chinese Academy of Sciences, Urumqi 830011, Xinjiang, P. R. China*

⁴*INAF – Osservatorio Astrofisico di Catania, Via S. Sofia 78, I-95123 Catania, Italy*

ABSTRACT

Asteroseismology of member pulsators provides a robust physical constraint on cluster parameters by linking internal stellar structures to the global properties of the host cluster. However, the parameters of NGC 1647 remains poorly constrained due to limited investigation, a situation that cluster asteroseismology can significantly refine. In this study, we identified 271 high-confidential cluster members in NGC 1647, using HDBSCAN clustering with radial-velocity validation. Its initial age is determined in the range of ~ 125 – 280 Myr, derived from isochrone fitting based on multi-survey metallicities (LAMOST, APOGEE, and NOT) and extinction-corrected Gaia photometry. Among the members, we found 96 periodic variables from *TESS* and *K2* photometry, including nine p -mode pulsators (five δ Sct and four hybrid δ Sct– γ Dor stars). Assuming a common cluster age and initial chemical composition, joint asteroseismic modeling is performed based on measured large frequency separations and individual mode frequencies. This yields a metallicity of $[\text{Fe}/\text{H}] = -0.08_{-0.01}^{+0.04}$, well consistent with the spectroscopic determinations, and a seismic age of 178_{-9}^{+11} Myr, more precise than isochrone-based estimates. This work shows the diagnostic potential of δ Sct asteroseismology in young open clusters and establishes a high-precision benchmark for future studies of NGC 1647 and other open clusters.

Keywords: asteroseismology – stars: variables : δ Scuti – open clusters and associations: general

1. INTRODUCTION

Open clusters, as the birthplaces of many stars in the Galaxy, provide ideal astrophysical laboratories for studying stellar formation and evolution (C. J. Lada & E. A. Lada 2003). Their member stars share, to the first order, a common age, distance, and initial chemical composition, thereby providing strong constraints on stellar models and evolutionary theory (A. S. M. Buckner & D. Froebrich 2014). Numerous studies have taken advantage of these properties to investigate different types of stars in open clusters. For example, J. A. Guzik et al. (2023) analyzed blue straggler stars in NGC 6819 based on space-based photometry; M. A. Ruíz Díaz et al. (2025) focused on B-type stars in the open cluster NGC 6834; and I. Berry et al. (2025) explored the occurrence rate of δ Scuti pulsators in NGC 3532. Conversely, many works have used specific stellar populations within clusters to constrain the global cluster parameters them-

selves. For instance, δ Scuti stars have been used to date young open clusters such as Trumpler 10 and Praesepe (D. Pamos Ortega et al. 2023); rotational sequences of fast rotators have provided an alternative age diagnostic for NGC 2281 (D. J. Fritzewski et al. 2023); and eclipsing binary systems have been employed to determine the age and distance of NGC 2506 (K. Yakut et al. 2025).

Asteroseismology has opened a new window for studying stellar clusters (e.g., D. Moździerski et al. 2019). Early ground-based studies, such as those by T. Arentoft et al. (1998) and T. Arentoft et al. (2005), provided initial asteroseismic insights into open clusters. The field has been revolutionized by high-precision, long-baseline time-domain photometry from space missions. D. Stello et al. (2010) utilized one month of *Kepler* photometry of NGC 6791 and NGC 6819 to perform the asteroseismic analysis of open clusters, highlighting the unique potential of *Kepler* (W. J. Borucki et al. 2010; S. B. Howell et al. 2014) for this field. Since then, intensive studies have focused on different types of pulsating stars to conduct asteroseismic investigations of open clusters. For

example, K. Brogaard et al. (2023) analyzed red giants in NGC 6866 to derive an asteroseismic age, while G. Li et al. (2025) constrained the age of NGC 2516 using g -mode pulsators. Widely distributed across open clusters, δ Scuti stars are frequently utilized and serve as important probes for young and intermediate-age systems. They have been increasingly incorporated into asteroseismic investigations of various open clusters (D. Pamos Ortega et al. 2023; D. B. Palakkatharappil & O. L. Creevey 2023). These studies demonstrate that asteroseismology of δ Scutis serves as an effective approach for refining the fundamental parameters of clusters, providing a robust check on ages derived from other methods.

NGC 1647 is an open cluster that exemplifies the challenges of precise parameters determination using traditional techniques. Situated beyond the Taurus dark cloud complex (J. Zdanavičius et al. 2005), its center is located at an RA of 71.48° and a Dec of 19.08° (J2000.0), at a distance of approximately 586.7 pc (T. Cantat-Gaudin et al. 2018). A notable disparity exists in recent age determinations for NGC 1647; estimates around ~ 260 Myr (see, e.g., W. S. Dias et al. 2021) diverge significantly from results near 360–390 Myr reported by other independent studies (e.g., T. Cantat-Gaudin et al. 2020; R. Carrera et al. 2022; Y. Tarricq et al. 2022). These substantial discrepancies, likely arising from variations in membership determinations, reddening corrections, and the choice of stellar models, underscore the ongoing uncertainty regarding the age of NGC 1647. This ambiguity motivates the necessity for an independent and more precise age determination using asteroseismology, which can also constrain other fundamental parameters (e.g., metallicity) that remain poorly investigated.

In this study, we present a precise determination of the fundamental parameters for NGC 1647 by applying asteroseismic analysis to its population of p -mode pulsators. Combining high-precision photometry from the $K2$ and $TESS$ with spectroscopic observation data from LAMOST, we utilize the large frequency separations ($\Delta\nu$, the characteristic spacing between consecutive radial modes; C. Aerts et al. 2010) and frequencies of the δ Scuti stars to derive a precise and independent age for this cluster. The structure of this paper is as follows: Section 2 details the membership selection process. Section 3 describes the determination of fundamental cluster parameters, including extinction and metallicity, alongside traditional isochrone fitting. In Section 4, we characterize the periodic variables identified among the cluster members. Section 5 provides a comprehensive account of the asteroseismic modeling

and age inference. We present a detailed discussion of our asteroseismic results in Section 6, focusing on the determination of cluster age and metallicity. Finally, our findings and conclusions are summarized in Section 7.

2. MEMBERSHIP DETERMINATION

2.1. Initial Data Determination and Clustering with HDBSCAN

The robust determination of member stars is fundamental to open cluster research, which ensures a more accurate determination of cluster parameters. The unprecedented high-precision astrometry from Gaia DR3 (Gaia Collaboration et al. 2023) enabled an accurate and comprehensive member determination for NGC 1647. We first adopted the central coordinates of RA = 71.48° , Dec = 19.08° (J2000.0) and a mean parallax of 1.68 mas for NGC 1647, as documented in T. Cantat-Gaudin et al. (2018). Then all stars were selected as potential members if they were within 100 pc centered around the central coordinates above. To exclude low-quality members, we selected sources with a signal-to-noise ratio (SNR) greater than 10 in the parallax and in each of the Gaia photometric bands (G, BP, and RP). In addition, we corrected the zero-point offsets of parallax for all sources, following the procedure described by L. Lindegren et al. (2021). These processes yielded an preliminary sample of 40,070 stars, hereafter referred as Sample 1.

Member stars of an open cluster should originate from the same parent molecular cloud and, consequently, exhibit significant overdensity in both spatial and kinematic spaces. To identify these coherent stellar populations, we employed the HDBSCAN algorithm (*Hierarchical Density-Based Spatial Clustering of Applications with Noise*; R. J. G. B. Campello et al. 2013; L. McInnes et al. 2017), which is effective at detecting cluster members within complex and noisy backgrounds. By extending the classical DBSCAN approach, it constructs a cluster hierarchy and extracts the most stable structures based on their persistence across multiple scales. A key advantage of HDBSCAN is its ability to operate without a fixed density threshold, making it robust against irregular stellar distributions often encountered in astrometric data. The algorithm’s performance is mainly governed by two parameters: `min_cluster_size`, which sets the minimum threshold for a group of stars to be considered a cluster, and `min_samples`, which dictates the algorithm’s sensitivity to local noise and outliers.

In our analysis, we applied HDBSCAN to Sample 1 with a five-dimensional phase space consisting of sky positions (α , δ), parallax (ϖ), and proper motions (μ_{α^*} , μ_{δ}). Following the configuration suggested by Y. Tarricq

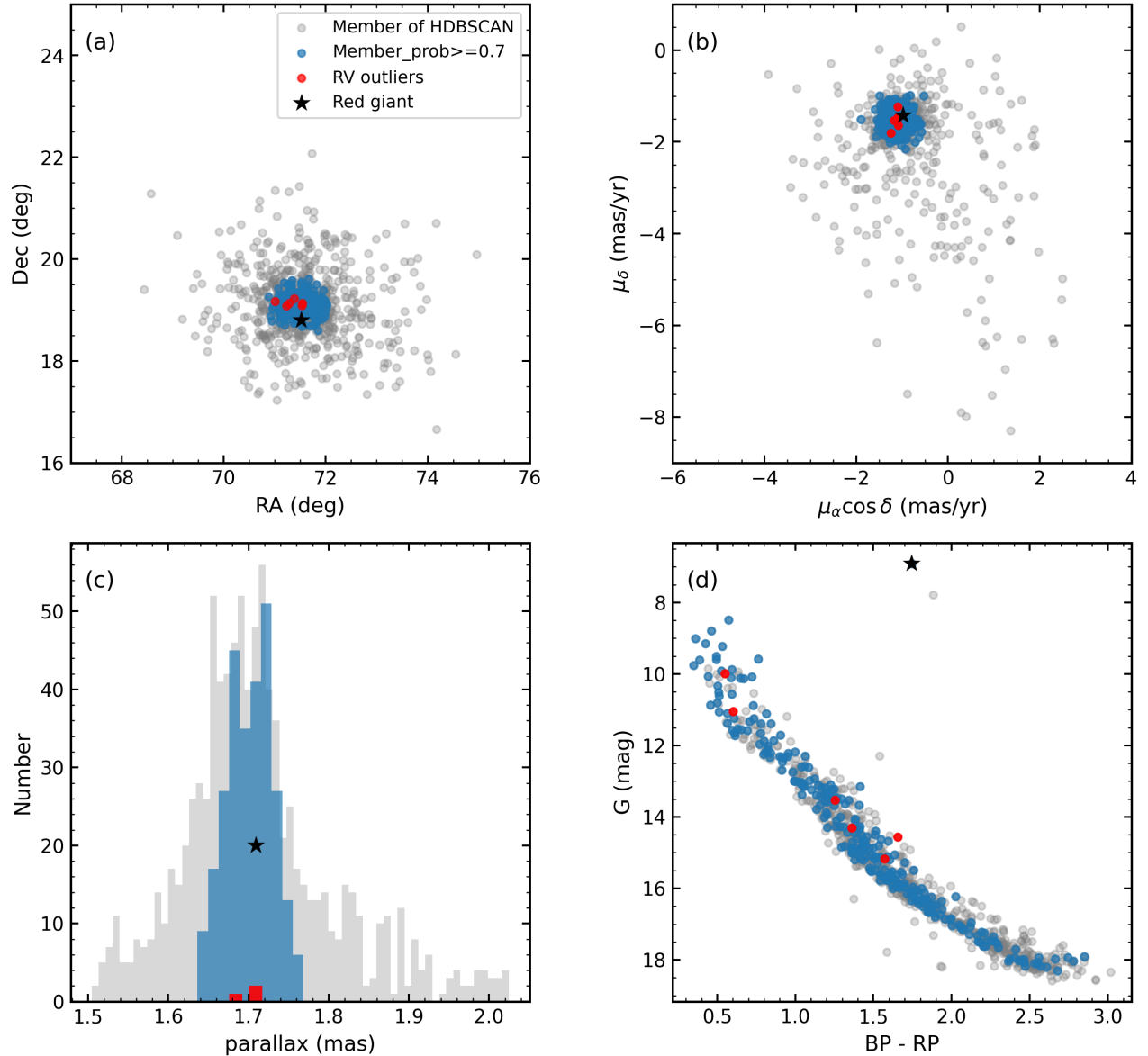


Figure 1. Membership selection for NGC 1647. Panel (a) shows the spatial sky distribution (RA vs. Dec), and panel (b) presents the proper motion diagram ($\mu_\alpha \cos \delta$ vs. μ_δ); Panel (c) displays the parallax distribution, while panel (d) shows the color–magnitude diagram (CMD, G vs. $G_{BP} - G_{RP}$). In these panels, grey points (or bars) represent all potential sources identified by HDBSCAN, blue denotes candidate members with membership probabilities $P \geq 0.7$, and red highlights RV outliers. The black star denotes the red giant star in NGC 1647.

et al. (2022), we set `min_cluster_size` to 40 and `min_samples` to 25. This procedure identified a prominent overdensity corresponding to the spatial and kinematic signature of NGC 1647. From the clustering output, we initially extracted a group of 931 stars associated with the primary cluster components, designated as Sample 2. As shown in Figures 1 (a)–(c), the distribution of Sample 2 appears relatively extended in both the celestial and kinematic parameter spaces. Furthermore, in the color–magnitude diagram (CMD; Figure 1 (d)),

several stars in this sample deviate significantly from the main-sequence (MS) locus. These features suggest that a fraction of field contaminants or low-probability members that the initial clustering could not fully exclude in Sample 2. To refine the sample, we utilized the membership probabilities (P) assigned by HDBSCAN. Following the criteria established in previous studies (Y. Tarricq et al. 2022; E. L. Hunt & S. Reffert 2023), stars with $P \geq 0.7$ were selected as reliable cluster candidates, which returns a sample of 277 member stars. Compared

to the initial clustering output, these candidates (colorful dots) show a significantly more concentrated distribution in all parameter spaces as shown in Figure 1, underscoring their high reliability as intrinsic members of NGC 1647.

2.2. Cleaning and Validation of Candidate Members

Although radial velocity (RV) measurements were not included in the initial HDBSCAN clustering due to incomplete data coverage, we utilized available RV information as an independent constraint to further refine our member determination. Theoretically, intrinsic member stars of an open cluster should exhibit consistent RVs reflecting the cluster’s bulk motion. To this end, we incorporated RV measurements from three independent sources: *Gaia* DR3, LAMOST DR12 low-resolution spectra (LRS; X.-Q. Cui et al. 2012; G. Zhao et al. 2012), and LAMOST DR12 medium-resolution spectra (MRS; C. Liu et al. 2020)¹. These datasets provided RV information for 144, 66, and 35 stars in our candidate list, respectively. As illustrated in Figure 2, the RV distribution for each source was fitted with a separate Gaussian function. Visually, a systematic offset of $\sim 5.5\text{--}6\text{ km s}^{-1}$ is evident in the LAMOST LRS distribution relative to the *Gaia* DR3 and MRS samples. This shift is consistent with the documented radial velocity zero-point (RVZP) offsets inherent in the LRS pipeline (see details in W. Zong et al. 2020). To account for this known instrumental characteristic, we applied a 5σ clipping threshold relative to the fitted mean (μ) of each independent dataset, as indicated by the shaded red regions in Figure 2. By centering the selection window on each survey’s specific peak, we ensure that the global zero-point shift does not bias our outlier identification. Consequently, stars falling within the 5σ range were retained, while others discarded. This process eliminated 4 stars from the *Gaia* DR3 sample and 2 stars from the LAMOST LRS sample (no outliers from the MRS sample).

Following the removal of these kinematic outliers, we finally established a catalog of 271 high-confidence member stars for NGC 1647. The coordinates and membership probabilities of these stars are summarized in Table 1. As shown in Figure 1(d), the CMD of these high-confidence members reveals a remarkably clear and coherent stellar sequence, which serves as a visual testament to the robustness of our membership selection. To further validate our results, we compared our final sample with the census provided by E. L. Hunt & S. Reffert (2023), who identified 360 cluster members with prob-

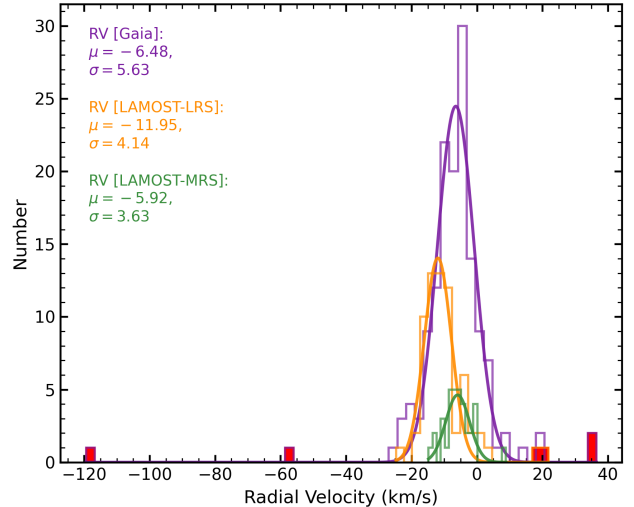


Figure 2. Radial velocity (RV) distributions and Gaussian fitting for NGC 1647. The shaded red regions highlight stars located beyond the 5σ clipping threshold, which are identified as RV outliers and excluded from the member list.

abilities $P \geq 0.7$. We find 258 common stars to theirs, with a substantial overlap, validating the robustness of our identified members.

3. ISOCHRONE FITTING OF NGC 1647

3.1. Metallicity Estimation and Extinction Correction

To estimate the metallicity of NGC 1647, we first utilized MRS spectra ($R \approx 7500$) from the LAMOST LK-MRS project (W. Zong et al. 2020; J.-N. Fu et al. 2020). We identified 25 coadded spectra with $SNR > 20$, a threshold that merits the precision required for robust parameter determination, as established by M. Qin et al. (2025). For stars with multiple measurements, we derived a weighted average metallicity, employing weights defined as $w_i = 1/\sigma_i^2$, where σ_i represents the uncertainty of each individual measurement. This process resulted in $[\text{Fe}/\text{H}]$ estimates for 17 member stars. Additionally, one member star has metallicity derived from one APOGEE high-resolution spectrum ($R = 22\,500$; SDSS Collaboration et al. 2025), while another from high-resolution spectra ($R = 67\,000$) using the Fibre-fed Echelle Spectrograph at the Nordic Optical Telescope (NOT; R. Carrera et al. 2022). Metallicity measurements were thus available for a total of 19 stars.

We then calculated the average value for the metallicity of NGC 1647 with associated uncertainty, based on a weighted formalism (see details of Eqn. 1 and 2 in W. Zong et al. 2020). Accounting for both measurement errors and stellar dispersion, this method provides a representative $[\text{Fe}/\text{H}] = -0.028 \pm 0.021$ dex for the cluster. Figure 3 displays the mean $[\text{Fe}/\text{H}]$ value relative to the

¹ <http://www.lamost.org/dr12/v1.0/>

Table 1. Member candidates of NGC 1647.

Gaia Source	RA(J2000.0)	Dec(J2000.0)	M_G	BP-RP	EPIC	TIC	Variable
3410096353900556544	71.04767122	19.22136916	2.6359	0.5807	247157739	18376371	gamma dor
3410077451747880704	70.96937553	19.09084764	2.4674	0.3416	247144102	18376451	
3410075527602535424	70.94892668	19.03029563	3.2697	0.6476	247137766	18376493	gamma dor
3410073126717441536	71.04618204	19.01216284	5.6582	1.2472	—	18376504	—
3409693516031329280	70.93836614	18.79058415	2.9270	0.5772	—	18376659	—
3410126139497593600	71.30860440	19.51081804	8.5904	1.9643	—	18437592	—
3410126246872879232	71.25140470	19.49799426	6.9106	1.3821	—	18437618	—
3410111025508793984	71.29381869	19.37287249	6.4750	1.2833	—	18437920	—
3410111055571988096	71.26242450	19.36893355	2.3703	0.3237	247173226	18437922	—
3410110338314042368	71.22452827	19.30452092	7.8618	1.7904	—	18438091	—
3410109376241364096	71.28719944	19.28825630	4.8800	1.0548	247164884	18438137	rotating
...

Notes. Column 1 lists the Gaia source ID for each target, while Columns 2 and 3 give the celestial coordinates (RA and Decl.; J2000.0). Columns 4 and 5 provide the extinction-corrected absolute G -band magnitude and the dereddened BP-RP color. Columns 6 and 7 list the K2 (EPIC) and TESS (TIC) identifiers, respectively. The final column indicates the variability classification of each star. Missing entries are marked with “—”. The complete version of this table will be made available online in a machine-readable format.

dispersion of the 19 member stars. The majority of the members lie well within the $\pm 3\sigma$ confidence interval, indicated by the shaded region. In contrast, only two outliers fall outside these confidence limits, even when their individual uncertainties are accounted for.

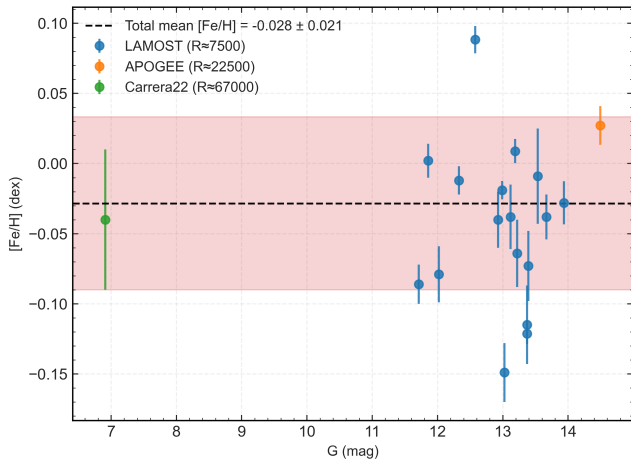


Figure 3. Metallicity as a function of magnitude for stars in NGC 1647. Blue dots represent data from the LAMOST MRS, the orange circle denotes the APOGEE measurement, and the green circle corresponds to the data from R. Carrera et al. (2022). Error bars indicate the reported uncertainties. The black dashed line marks the weighted mean metallicity, and the pink shaded region represents the $\pm 3\sigma$ confidence interval around the mean.

To account for the interstellar extinction, we adopted a color excess of $E(B - V) = 0.35$, as determined by C. A. Guerrero et al. (2011) via multi-band photometry. The extinction within the *Gaia* passbands was

computed following the formalism of C. Danielski et al. (2018), which relates the monochromatic extinction A_0 at 550 nm to the band-specific extinction (e.g., A_G) through the following expression:

$$\frac{A_G}{A_0} = a_1 + a_2X + a_3X^2 + a_4X^3 + a_5A_0 + a_6A_0^2 + a_7A_0^3 + a_8A_0X + a_9X^2A_0 + a_{10}XA_0^2, \quad (1)$$

where X represents the intrinsic color index $(G_{BP} - G_{RP})_0$, and the coefficients $a_1 - a_{10}$ are specific to the *Gaia* DR3 photometric system (M. Riello et al. 2021)². The absolute magnitudes and intrinsic colors for each member star were subsequently derived by combining individual *Gaia* parallaxes with the calculated extinction values. The resulting de-reddened CMD is presented in Figure 4 (a).

3.2. Isochrone Fitting

The age of NGC 1647 was constrained via isochrone fitting based on the MIST stellar evolutionary models (A. Dotter 2016; J. Choi et al. 2016; B. Paxton et al. 2011, 2013, 2015, 2018), with input of $[\text{Fe}/\text{H}] = -0.03$ dex. This choice is a compromise between the density of MIST grid with the metallicity resolution of 0.01 dex and the $[\text{Fe}/\text{H}] = -0.028$ dex determined by spectroscopy. The model grid spans $\log(\text{Age}/\text{yr}) = 5.0 - 10.3$ in steps of 0.05.

To quantify the goodness-of-fit, we employed the squared Euclidean distance, d^2 , between extinction-

² <https://www.cosmos.esa.int/web/gaia/edr3-extinction-law>

corrected magnitude and color index for each star and its nearest neighbor on a theoretical isochrone in the M_G vs. $(G_{\text{BP}} - G_{\text{RP}})_0$ plane (L. Liu & X. Pang 2019). Specifically, to enhance the sensitivity of the age determination and minimize the influence of low-mass stars, the d^2 parameter was calculated by restricting the sample to 64 bright stars with $M_G < 3$ mag. The goodness-of-fit parameter is defined as:

$$d^2 = \frac{1}{N} \sum_{i=1}^N [\Delta M_{G,i}^2 + \Delta(G_{\text{BP}} - G_{\text{RP}})_{0,i}^2], \quad (2)$$

where N is the number of stars, and the differences Δ represent the distance to the nearest neighbor along the isochrone, identified via a k -d tree nearest-neighbor search (J. L. Bentley 1975).

Figure 4 (a) presents the CMD of NGC 1647. The cluster exhibits a clear Extended Main Sequence Turn-off (eMSTO) phenomenon at the bright end, and its main sequence (MS) shows a significant width broadening, which we quantify by measuring its vertical and horizontal extents as indicated by the black line segments in the figure, yielding $\Delta G \approx 1.33$ and $\Delta(G_{\text{BP}} - G_{\text{RP}}) \approx 0.26$. The observed spread likely arises from a combination of photometric uncertainties, differential reddening, and a high fraction of unresolved binaries. To mitigate the systematic bias toward older ages typically induced by these phenomena, we opted against relying on a single minimum- d^2 solution. Instead, we examined a suite of best-fitting isochrones with $d^2 < 0.05$. As shown in the zoom-in panel of Figure 4 (a), the d^2 values for models within the range of $\log(\text{age}/\text{yr}) = 8.10$ – 8.45 (~ 125 – 280 Myr) remain very similar. No significant visual distinction can be made among these isochrones in the turn-off region. This dispersion, likely driven by the eMSTO effect, results in a relatively broad age constraint when relying solely on CMD-based isochrone fitting. Furthermore, the low sensitivity of isochrone morphology to age within the MSTO region, coupled with variations in adopted metallicities and extinction corrections, likely explains the discrepant age estimates reported in previous studies, such as 256 Myr (W. S. Dias et al. 2021) and 390 Myr (R. Carrera et al. 2022).

4. VARIABLE STARS IN NGC 1647

4.1. Photometric Analysis

NGC 1647 is observed by *K2* Campaign 13 with available photometry for 56 member stars, whose light curves were retrieved from the Mikulski Archive for Space Telescopes (MAST) (STScI 2016) via the `Lightkurve` package (Lightkurve Collaboration et al. 2018). For *TESS*, the available SPOC light curves (D. A. Caldwell et al.

2020) for 172 member stars were retrieved from MAST (TESS Team 2021), as they were observed through Sectors 43-44 and 70-71. All those light curves are processed through the `Lightkurve` package (Lightkurve Collaboration et al. 2018), including outlier rejection via a local 3σ moving clipping algorithm and the `flatten` routine from the `wotan` package (M. Hippke et al. 2019) to remove long-term trends. The light curves from different sectors were concatenated and normalized to produce a continuous time series photometry. Further details of these procedures are provided in K. Xing et al. (2024). Finally, we computed the Lomb-Scargle periodogram (N. R. Lomb 1976; J. D. Scargle 1982) for each assembled light curve, which were utilized to characterize the variability properties.

To further characterize the variability properties, variable candidates were cross-matched with *Gaia* DR3 to construct a CMD. Their positions on CMD were compared against the theoretical and empirical instability strips for δ Scuti and γ Doradus stars (M. A. Dupret et al. 2005; S. J. Murphy et al. 2019). We note that the instability strip boundaries were transformed from the $T_{\text{eff}}-L$ plane into extinction-corrected $(G_{\text{BP}} - G_{\text{RP}})_0$ colors and absolute M_G magnitudes accounting for bolometric corrections and interstellar extinction (M. Riello et al. 2021). These strips were subsequently superimposed on the CMD for a direct comparison between the observed stellar variability and theoretical predictions.

4.2. Identification and Classification of Variable Stars

The variability of each target was characterized by combining the frequency analysis of its light curve with its evolutionary stage on the CMD. We identified 96 periodic variables and assigned them to specific classifications. The sample is dominated by 65 rotational variables, with the remaining fraction comprising various types of pulsators and eclipsing binaries. Figure 4 (b) presents their distribution on the CMD with their classifications labelled, while Figure 4 (c) provides characteristic light curve segments for each class with *TESS* and *K2* photometry. We describe each group of variables in detail as follows.

Slowly Pulsating B-type (SPB) stars. SPB represents a distinct class of early-type variables, exhibiting multiperiodic, high-radial-order g -mode pulsations. These oscillations provide a window into stellar interior, enabling precise constraints on internal rotation and mixing processes (C. Waelkens 1991). Two members of NGC 1647, TIC 18442268 and TIC 18442894, are identified as SPB stars. While the former was previously categorized as a δ Sct, γ Dor, or SX Phe candidate (N. Mowlavi et al. 2023), its location above those

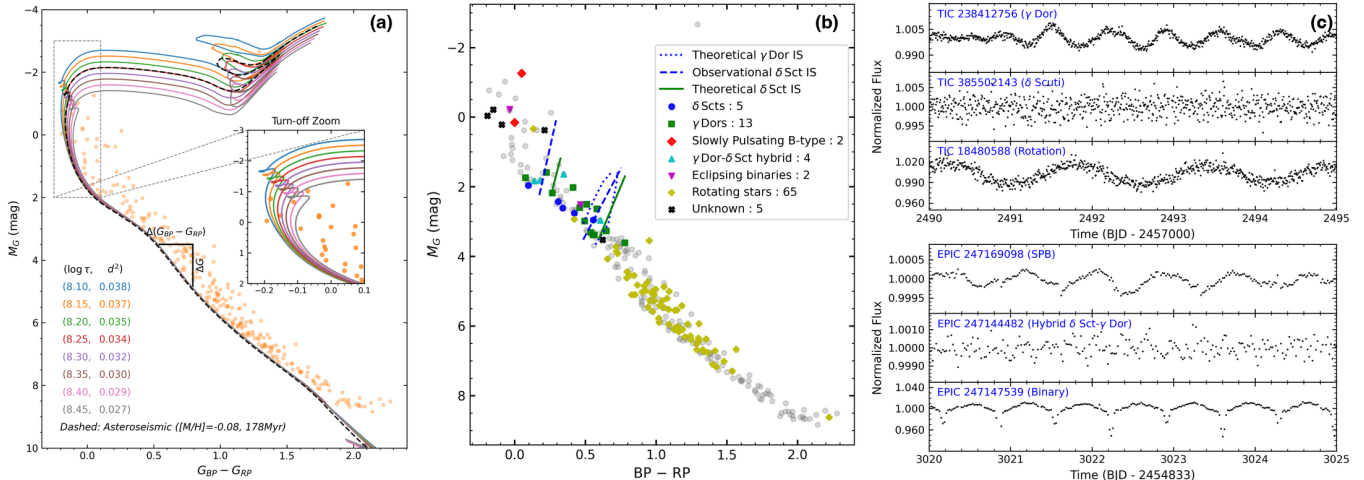


Figure 4. Isochrone fitting and variable stars in NGC 1647. (a) Isochrone fitting for NGC 1647. Orange points represent extinction-corrected member stars. The solid curves show the eight best-fitting MIST isochrones, where τ denotes the age of the isochrones. (b) CMD of the member stars in NGC 1647. Different symbols represent the various types of variable stars identified in this study. The blue dashed and dotted curves indicate the theoretical and empirical instability strips of γ Dor and δ Sct stars, respectively. (c) Representative segments of the light curves for the six types of variable stars identified in NGC 1647. The top three panels display *TESS* data, while the bottom three panels present observations from the *K2* mission.

instability strips and the presence of low-frequency g -mode pulsations favor its reclassification as an SPB star. TIC 18442894, situated near the upper main sequence, is a new identification from this work.

γ Doradus stars. We discovered 13 new γ Doradus variables as members of NGC 1647. Their amplitude spectra exhibit low-frequency g -mode pulsations characteristic of γ Dor stars (M. A. Dupret et al. 2005; T. Van Reeth et al. 2015). While a few candidates are situated slightly outside the theoretical instability strip, these deviations likely stem from residual uncertainties in interstellar extinction and photometry. Similar discrepant cases have been reported in previous cluster studies, potentially linked to enhanced metallicities and unresolved binary components (G. Li et al. 2020).

δ Scuti stars. Five new δ Scuti stars were identified, exhibiting high-frequency p -mode pulsations characteristic of this variable class (S. J. Murphy et al. 2019). Additionally, three new δ Sct- γ Dor hybrid stars were discovered, dominated by high-frequency p -modes alongside lower-amplitude g -modes, while an additional hybrid pulsator shows comparable amplitudes in both frequency range. These stars are situated within the overlapping region of the δ Sct and γ Dor instability strips, a domain where both the κ -mechanism and convective blocking are effectively operative (A. Grigahcène et al. 2010).

Eclipsing binaries. Two eclipsing binary systems were identified: EPIC 247147539 and TIC 18479179. Both are listed in the *Gaia* catalogue of eclipsing binary can-

didates (N. Mowlavi et al. 2023), the orbital periods of them is 1.37 and 12.23 day, respectively.

Rotational modulation variables. Their periodic brightness variations originate from surface inhomogeneities, such as starspots, which rotate in and out of the line of sight (A. McQuillan et al. 2014). A sample of 65 stars exhibit sinusoidal or quasi-sinusoidal variations, consistent with rotational modulation induced by starspots. The derived rotation periods establish a foundation for gyrochronological dating of NGC 1647, which will be explored in a forthcoming paper.

Unclassified variables. Five stars are identified as variables but defy specific classification with the available photometry.

5. ASTEROSEISMOLOGY OF δ SCUTI STARS

5.1. Mode identification

Following the classification in Section 4, we identified nine p -mode pulsators in NGC 1647, comprising five classical δ Scuti stars and four δ Sct- γ Dor hybrid pulsators. Their fundamental properties, including *Gaia* DR3 astrometry and photometry, are summarized in Table 2. In δ Scuti stars, p -mode frequencies often exceed the Nyquist limit of Kepler long-cadence photometry, giving rise to potential aliasing artifacts known as super-Nyquist frequencies (SNFs; S. J. Murphy et al. 2013; X. Wang et al. 2025). To preclude ambiguities in mode identification and ensure the detection of real pulsation signals, we restrict our analysis to *TESS* short-cadence photometry.

Table 2. Astrometric and photometric parameters of the 9 target stars in NGC 1647.

TIC ID	RA (deg)	Dec (deg)	Parallax (mas)	$\mu_\alpha \cos \delta$ (mas yr ⁻¹)	μ_δ (mas yr ⁻¹)	G (mag)	$BP - RP$ (mag)	M_G (mag)
18438742	71.2558	19.0406	1.729	-1.084	-1.471	12.611	1.085	2.966
18442420	71.3592	19.0945	1.668	-0.895	-1.938	11.394	0.844	1.635
18478821	71.5460	19.3013	1.684	-1.571	-1.886	12.174	0.810	2.431
18479154	71.5448	18.9735	1.719	-0.808	-1.741	11.559	0.655	1.835
18480650	71.6381	18.9810	1.695	-0.940	-1.942	11.722	0.614	1.962
18480935	71.6072	19.2447	1.702	-1.276	-1.804	12.464	0.915	2.760
18540036	71.9499	19.3833	1.680	-0.932	-1.287	11.581	0.691	1.814
18547844	72.0023	19.0241	1.704	-1.062	-1.438	12.327	0.839	2.613
385502143	71.1643	19.2234	1.738	-1.175	-1.470	12.598	1.038	2.958

NOTE—Astrometric and photometric parameters (RA, Dec, Parallax, Proper Motions, G magnitude, and $BP - RP$ color) are retrieved from Gaia DR3. The last column lists the absolute magnitudes obtained in Section 3.1.

We performed frequency extraction using the `MultiModes` package (D. Pamos Ortega et al. 2022), an automated pre-whitening tool specifically designed for the frequency analysis of space-based photometry. To analyze the extracted frequencies, we searched for regular frequency patterns, such as the distinct ridge structures revealed in échelle diagrams. Recent studies have shown that these patterns are frequently observed in young δ Sct stars (T. R. Bedding et al. 2020; A. Gautam et al. 2025), offering crucial information to stellar interior. These regularities provide stringent observational constraints necessary for identifying radial ($\ell = 0$) and low-degree non-radial ($\ell = 1, 2, 3$) modes.

Then échelle diagrams of these nine targets were constructed with the `échelle` Python package (D. Hey & W. Ball 2020). We have successfully identified five stars exhibiting regular frequency spacings, which we interpret as the large frequency separation ($\Delta\nu$); these targets include TIC 18442420, TIC 18438742, TIC 18480935, TIC 18547844, and TIC 385502143. Using these $\Delta\nu$ values, we performed mode identification for each star, with the identified $\ell = 0$ and $\ell = 1$ frequencies. After this initial observational identification, we further refined the mode identification by iteratively comparing the observed frequency spectra with the theoretical models described in Section 5. In particular, three frequencies in TIC 18438742 and TIC 385502143 were identified as $\ell = 2$ and $\ell = 3$ modes, primarily based on their agreement with the predicted frequency patterns of the best-fitting models. The identified modes, as marked in Figure 5, correspond to the dominant peaks in the spectra and serve as the basis for our asteroseismic modeling. The remaining peaks, some of which exhibit considerable amplitude, are attributed to phenomena such as rotational splitting, modes of

higher spherical degree, or the intrinsic mode crowding characteristic of δ Sct stars (S. J. Murphy et al. 2022).

However, as illustrated in Figure 5, only a limited number of frequencies could be definitively identified for each star. Relying on such sparse frequency sets to constrain asteroseismic models may result in large parameter uncertainties for individual targets. Considering these five pulsators are members of NGC 1647 with a common age and initial chemical composition, we can jointly model these stars by utilizing the 28 identified frequencies and their respective $\Delta\nu$ values as collective constraints. This ensemble approach provides more stringent and reliable estimates for the fundamental parameters of the cluster.

5.2. MESA model grid and joint fitting

Stellar evolutionary models were constructed using the `MESA` code (B. Paxton et al. 2011, 2013, 2015, 2018, 2019), with corresponding p -mode pulsation frequencies calculated via the `GYRE` package (R. H. D. Townsend & S. A. Teitler 2013; R. H. D. Townsend et al. 2018; M. Sun et al. 2023). A series model grid was established by spanning the primary stellar parameter space: mass $M \in [1.4, 2.5] M_\odot$ (step: $0.01 M_\odot$) and metallicity $[\text{Fe}/\text{H}] \in [-0.10, +0.04]$ dex (step: 0.01). This $[\text{Fe}/\text{H}]$ range, informed by the spectroscopic analysis in Section 3.1, covers the 3σ uncertainty interval, as denoted by the pink shaded region in Figure 3. For each evolutionary track, stellar ages, τ , were sampled up to 500 Myr with a 1 Myr resolution—a range that broadly covers the typical cluster ages reported in the literature ($\lesssim 400$ Myr). Other inputs in `MESA` remained at their default settings. For each model, the theoretical large frequency separation ($\Delta\nu_{\text{mod}}$) was derived via a linear fit to $\ell = 0$ modes with $n \geq 5$ (S. K. Panda et al. 2024); this criterion was extended to $n \geq 4$ in cases of sparse modes.

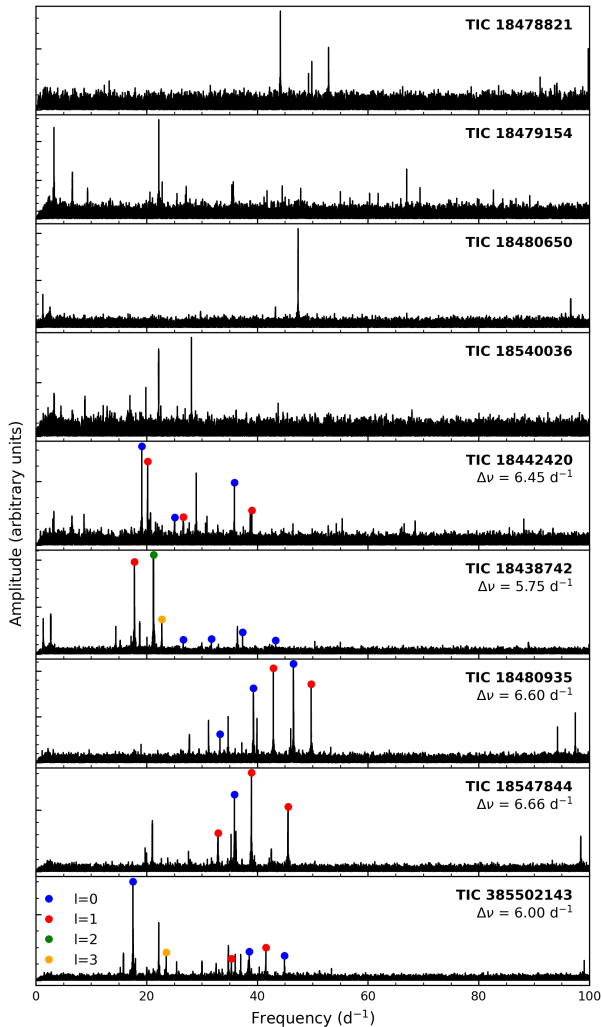


Figure 5. Amplitude spectra of the nine p -mode pulsators identified in NGC 1647 based on TESS light curves. The colored symbols denote pulsation modes with different spherical degrees: blue, red, green, and orange circles represent frequencies identified as $\ell = 0, 1, 2,$ and 3 modes, respectively. For stars exhibiting regular frequency patterns, the measured $\Delta\nu$ values are indicated in the corresponding panels.

The confirmed cluster membership of these five pulsators provides a unique advantage, enabling a joint fitting analysis by leveraging their coeval and chemically homogeneous nature as collective constraints. Within this framework, we explored the parameter space across a discrete grid of $([\text{Fe}/\text{H}], \tau)$ pairs. At each grid point, the stellar mass (M) for the j th star was treated as a local free parameter. To assess the model-data consistency, we calculated a χ^2 statistic for the j th star with

$N_{\text{obs},j}$ identified frequencies $(\nu_{\text{obs},j,i})$, defined as:

$$\chi_j^2([\text{Fe}/\text{H}], \tau; M) = \frac{(\Delta\nu_{\text{obs},j} - \Delta\nu_{\text{mod}})^2}{\sigma_{\Delta\nu}^2} + \frac{1}{N_{\text{obs},j}} \sum_{i=1}^{N_{\text{obs},j}} \frac{(\nu_{\text{obs},j,i} - \nu_{\text{mod,closest},i})^2}{\sigma_\nu^2}, \quad (3)$$

where $\nu_{\text{mod,closest},i}$ denotes the model frequency that best matches the i -th observed frequency for the given stellar parameters. Regarding the uncertainty terms, we adopt a conservative $\sigma_{\Delta\nu} = 0.2 \text{ d}^{-1}$, a value ten times the bin size of our échelle analysis. This accounts for the inherent ambiguity in identifying $\Delta\nu$ for these pulsators. For individual frequencies, we set $\sigma_\nu \approx 0.0185 \text{ d}^{-1}$, corresponding to the frequency resolution of two-sector *TESS* observations.

For each star, the best-fitting model mass at a given $([\text{Fe}/\text{H}], \tau)$ is determined by minimizing the individual χ^2 :

$$\chi_{j,\text{min}}^2([\text{Fe}/\text{H}], \tau) = \min_M [\chi_j^2([\text{Fe}/\text{H}], \tau; M)]. \quad (4)$$

The total χ^2 for each $([\text{Fe}/\text{H}], \tau)$ group is then computed by averaging the individual minima over the five pulsators:

$$\chi_{\text{tot}}^2([\text{Fe}/\text{H}], \tau) = \frac{1}{5} \sum_{j=1}^5 \chi_{j,\text{min}}^2([\text{Fe}/\text{H}], \tau). \quad (5)$$

This procedure is repeated across the entire $([\text{Fe}/\text{H}], \tau)$ grid to yield a comprehensive χ_{tot}^2 map, which serves as the basis for the subsequent statistical inference of the cluster's fundamental parameters.

5.3. Model Fitting Results

We construct a two-dimensional Kernel Density Estimation (KDE) in the $([\text{Fe}/\text{H}], \tau)$ parameter space, with each model weighted by its inverse- χ^2 value. As shown in Figure 6, the resulting distribution exhibits a single, prominent density peak, indicating that the pulsational constraints converge toward a unique solution in the $([\text{Fe}/\text{H}], \tau)$ plane. To determine the joint uncertainties of the cluster parameters $[\text{Fe}/\text{H}]$ and τ , we employ a likelihood-ratio test (Y. Avni 1976; S. K. Panda et al. 2024). By optimizing the stellar masses at each fixed $([\text{Fe}/\text{H}], \tau)$ grid point, we effectively marginalize their influence, allowing for a direct evaluation of the goodness of fit across the parameter plane. Assuming two degrees of freedom, the 3σ confidence region is defined by the contour $\chi_{\text{tot}}^2 \leq \chi_{\text{min}}^2 + 9.21$, marked by white dashed contour in Figure 6. Within this boundary, 101 models are retained, corresponding to approximately 1.06% of

Table 3. Comparison of observed and model frequencies for p -mode pulsators.

TIC	Observation			Best-fit Model			$ \delta\nu $ (d ⁻¹)	M_{model} (M_{\odot})
	ν_{obs} (d ⁻¹)	ℓ	$\Delta\nu_{\text{obs}}$ (d ⁻¹)	ν_{mod} (d ⁻¹)	ℓ, n	$\Delta\nu_{\text{mod}}$ (d ⁻¹)		
18438742	21.2522	2		21.6484	2, 1		0.3962	$2.46^{+0.01}_{-0.03}$
	17.8253	1		17.7827	1, 1		0.0426	
	22.7783	3		22.7045	3, 1		0.0738	
	37.3628	0	5.75	37.3651	0, 5	5.7230	0.0023	
	31.7056	0		31.9092	0, 4		0.2036	
	26.6204	0		26.9066	0, 3		0.2862	
	43.3006	0		43.0518	0, 6		0.2489	
18442420	19.1388	0		19.4816	0, 1		0.3429	$2.17^{+0.01}_{-0.04}$
	20.1908	1		20.0636	1, 1		0.1271	
	35.8703	0	6.45	35.9580	0, 4	6.45	0.0877	
	38.9969	1		38.8609	1, 4		0.1360	
	26.6129	1		26.3309	1, 2		0.2820	
	25.0714	0		25.0954	0, 2		0.0240	
18480935	46.5436	0		46.3147	0, 5		0.2289	$1.89^{+0.01}_{-0.05}$
	42.9043	1		42.7813	1, 4		0.1230	
	49.7456	1	6.60	49.7970	1, 5	6.88	0.0515	
	39.3147	0		39.5794	0, 4		0.2646	
	33.2759	0		33.4028	0, 3		0.1268	
18547844	38.9402	1		39.0264	1, 4		0.0862	$2.16^{+0.01}_{-0.03}$
	35.8646	0	6.66	36.1123	0, 4	6.47	0.2477	
	45.5543	1		45.4339	1, 5		0.1204	
	32.9036	1		32.6963	1, 3		0.2072	
385502143	17.5627	0		17.8805	0, 1		0.3178	$2.38^{+0.01}_{-0.04}$
	41.5496	1		41.5596	1, 5		0.0100	
	38.5756	0	6.00	38.7134	0, 5	5.93	0.1378	
	23.5534	3		23.4655	3, 1		0.0878	
	44.9238	0		44.6056	0, 6		0.3182	
	35.3245	1		35.6911	1, 4		0.3666	

Notes. Observed pulsational properties are compared with the best-fit model predictions. Columns 2–4 list the observed frequencies (ν_{obs}), identified spherical degrees (ℓ), and $\Delta\nu_{\text{obs}}$. Columns 5–7 provide the corresponding theoretical values, where ℓ and n denote the spherical degree and radial order, respectively. $|\delta\nu|$ represents the absolute frequency residual ($|\nu_{\text{obs}} - \nu_{\text{mod}}|$). The asteroseismic stellar masses (M_{model}) in the final column are derived from the 68% (1σ) HPD credible region of the joint fitting solution.

the lowest- χ^2 models in the grid, which defines the statistical confidence region around the best-fitting solution. We adopt the KDE peak values as the final cluster parameters. The associated uncertainties are derived from the 68% highest posterior density (HPD) credible interval, calculated within the 3σ confidence region. This corresponds to 69 models, from which we obtain: $\tau = 178^{+11}_{-9}$ Myr and $[\text{Fe}/\text{H}] = -0.08^{+0.04}_{-0.01}$ dex.

The performance of our best-fitting models is illustrated in Figure 7. In the top-right panel, the observed

frequencies (colored dots) are plotted against the theoretical predictions (black open circles). To provide a comprehensive view of the stellar parameters, the bottom axis indicates the model-derived stellar masses, while the top axis shows the corresponding theoretical absolute magnitudes in the G band (M_G). These M_G values were calculated by passing the model parameters through the synthetic photometry tool provided by Y.

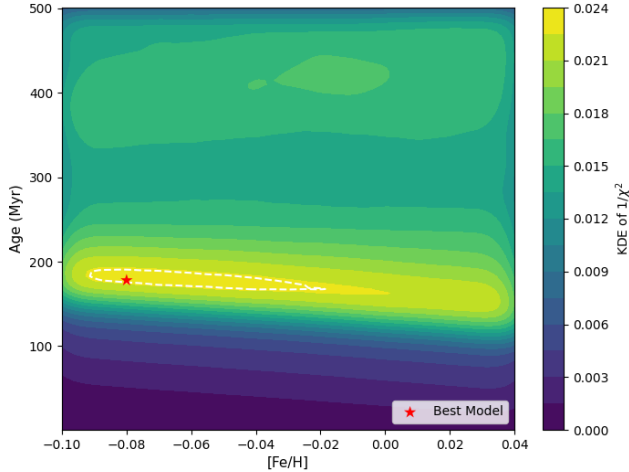


Figure 6. A two-dimensional Kernel Density Estimation (KDE) in the $([\text{Fe}/\text{H}], \tau)$ parameter space, with each model weighted by its inverse- χ^2 value. The white dashed contour marks the 3σ confidence region defined by $\chi_{\text{tot}}^2 \leq \chi_{\text{min}}^2 + 9.21$, and the red pentagram indicates the best-fitting model within the grid.

Chen et al. (2019)³. The observed frequencies agree well with the theoretical predictions, confirming the robustness of the joint fitting procedure.

As summarized in Table 3, the joint fitting procedure yields a robust asteroseismic solution for all five pulsators. Quantitatively, the individual frequencies (ν_{obs}) and large frequency separations ($\Delta\nu_{\text{obs}}$) show mean absolute differences of 0.18 d^{-1} and 0.10 d^{-1} relative to the model predictions, respectively. These residuals are comparable to the 0.2 d^{-1} resolution limit of the échelle analysis used for mode identification. Such consistency is visually manifested in Figure 7, where the majority of observed frequency peaks align precisely with the theoretical $\ell = 0$ and $\ell = 1$ ridges constructed using the model $\Delta\nu_{\text{mod}}$. By successfully recovering these ridge structures, the models not only confirm the observed spherical degrees ℓ but also provide the constraints to assign radial orders n for all identified modes. This agreement yields a self-consistent seismic solution for the pulsating members of NGC 1647.

A comparison between the Gaia absolute magnitudes in Table 2 (M_G) and the corresponding model-derived absolute magnitudes (G in Figure 7) reveals a noticeable discrepancy. For instance, TIC 18442420 and TIC 18547844 possess nearly identical model-predicted magnitudes (1.337 and 1.353 mag, respectively), whereas their observation-based absolute mag-

nitudes differ by approximately 1.0 mag ($M_G = 1.635$ and 2.613 mag, respectively). We note that the absolute magnitudes in Section 3.1 were derived assuming a single extinction value for the entire cluster. In this context, Frasca et al. (2026, submitted) found that A_V values in NGC 1647 exhibit a substantial range from 0.3 to 2.1 mag, which ($\Delta A_V \approx 1.8$ mag) can induce an average shift of approximately 1.3 mag in M_G and 0.8 mag in $(G_{BP} - G_{RP})$. This indicates that differential extinction may be a factor contributing to the discrepancy between the Gaia absolute magnitudes and the seismic model predictions.

6. DISCUSSION

Asteroseismology has proven to be a powerful tool for deriving precise fundamental parameters of open clusters (e.g., K. Brogaard et al. 2023; D. Pamos Ortega et al. 2023; D. B. Palakkatharappil & O. L. Creevey 2023; G. Li et al. 2025). NGC 1647 presents a diverse laboratory for such studies, hosting various types of pulsators including SPB stars, γ Doradus stars, and δ Scuti stars. However, current observational data dictate which of these can be effectively utilized as seismic probes. While SPB and γ Doradus stars offer unique insights into deep interiors via g -mode pulsations, their characteristic long periods require an observational baseline exceeding our current data to achieve the necessary frequency resolution. Furthermore, although a red giant member is identified in Figure 4 (b), no detectable solar-like oscillations were found in that light curve. Consequently, the short-period p -mode pulsations of the δ Scuti members are clearly resolved, making them the most robust and practical tools for refining the cluster’s fundamental parameters at this stage.

The presence of a red giant in such a young cluster warrants further discussion. The membership of this star is well supported by several independent indicators. Its Gaia DR3 astrometric parameters are consistent with those of the cluster members, and the membership probability is 0.88 (see Figure 1). In addition, its radial velocity ($RV = -6.74 \text{ km s}^{-1}$) is consistent with the cluster mean value ($-6.48 \pm 5.63 \text{ km s}^{-1}$). From an evolutionary perspective, its position on the CMD (Figure 4 (a)) agrees well with the best-fitting isochrone ($t \approx 178 \text{ Myr}$). The corresponding model mass at this evolutionary stage is about $4.17 M_{\odot}$, indicating that a mid-mass star in the cluster could have already evolved off the main sequence and reached the giant phase. Although this evolutionary stage is relatively short-lived, the presence of such a star is still compatible with the expected evolution of intermediate-mass stars in a $\sim 178 \text{ Myr}$ cluster. Therefore, although rare, the existence of

³ <https://sec.center/YBC/>

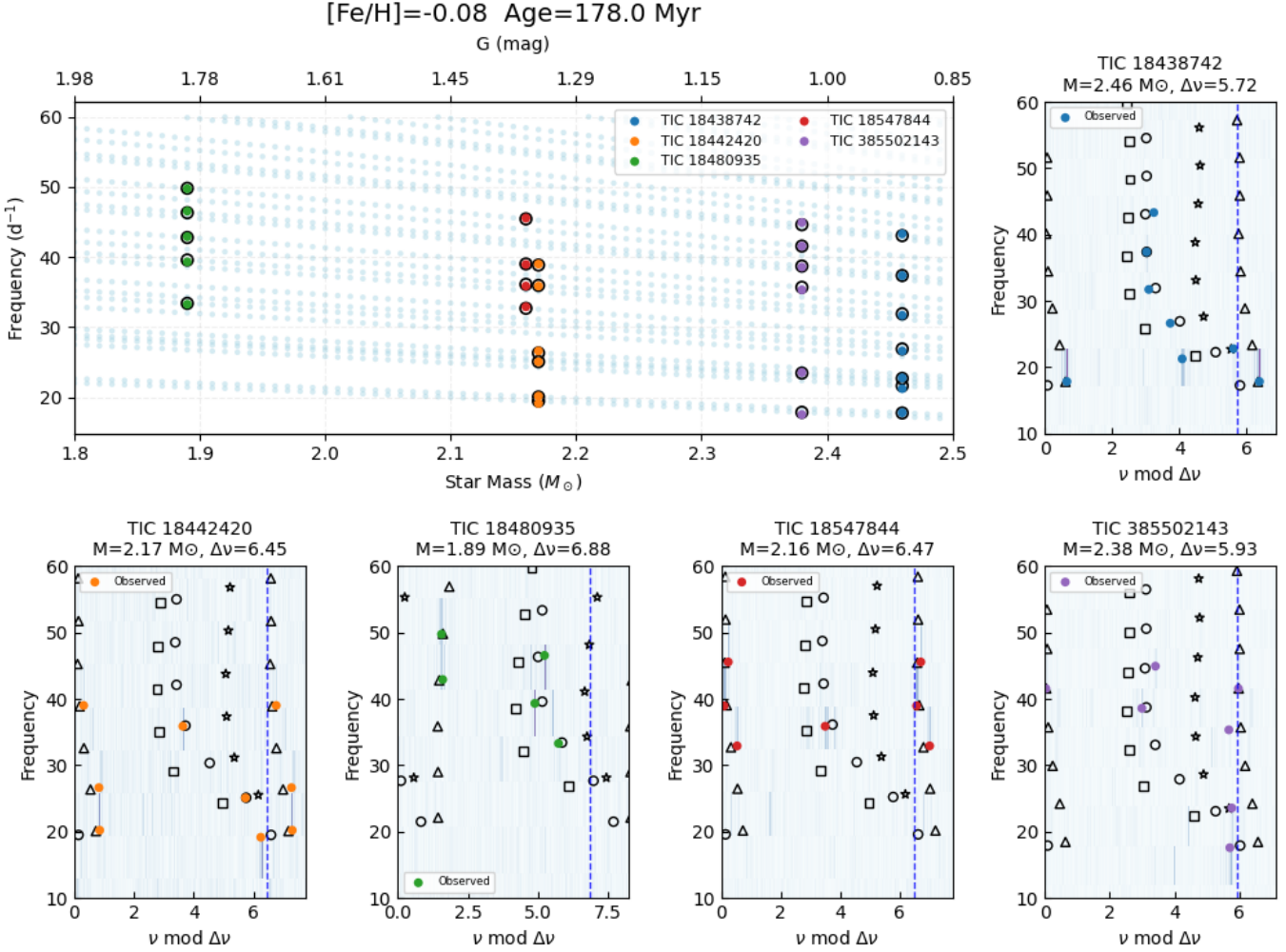


Figure 7. Comparison between the observed and modeled pulsation properties for the five pulsating members of NGC 1647. Top-right panel: comparison between the observed (filled symbols) and modeled (open symbols) pulsation frequencies for the best-fitting model of each star. The bottom horizontal axis shows the stellar mass, while the top horizontal axis indicates the corresponding Gaia G -band absolute magnitude derived from the models. Black open circles mark the model frequencies that best match each observed frequency. Top-left and bottom panels show the individual échelle diagrams for the five pulsators, where the observed frequencies (filled circles) and their closest matching model frequencies (open symbols) are plotted modulo $\Delta\nu$ and overlaid on the corresponding power spectra. Different symbols denote modes with different spherical degrees: circles ($l = 0$), triangles ($l = 1$), squares ($l = 2$), and stars ($l = 3$).

this red giant does not contradict the derived cluster age.

Our results for δ Scuti stars underscore the remarkable capability of asteroseismology to refine cluster parameters with high precision. As illustrated in Figure 4 (a), the isochrone corresponding to our best-fit asteroseismic age (178_{-9}^{+11} Myr) aligns well with the age interval independently determined via isochrone fitting in Section 3 (125–280 Myr). Similarly, the derived metallicity of $[\text{Fe}/\text{H}] = -0.07_{-0.01}^{+0.04}$ is consistent with the spectroscopic value obtained in Section 3.1. This dual-parameter agreement supports the robustness of the seismic solution. However, the model comparison shown in Figure 6

indicates that the pulsation frequencies are more sensitive to stellar age than to metallicity within the explored parameter range. Consequently, the relatively small uncertainty in $[\text{Fe}/\text{H}]$ mainly reflects the distribution of acceptable models within the adopted grid. Systematic uncertainties associated with the input physics of stellar models (e.g., opacities, mixing prescriptions, and convection overshooting) may introduce additional uncertainties in the derived cluster parameters that are not fully captured by the χ^2 analysis.

Among the possible sources of systematic uncertainties, stellar rotation and convective core overshooting can significantly affect both stellar evolution and pul-

sation properties. In the present work, we adopted a simplified grid of stellar models that does not include rotational effects or overshooting. For the five δ Scuti stars analyzed here, only TIC18547844 currently has a spectroscopic measurement of projected rotational velocity, with $v \sin i = 85.4 \text{ km s}^{-1}$ derived from LAMOST spectra. Several relatively high-amplitude frequencies in this star (e.g., 21.0544 d^{-1}) cannot be reliably reproduced by non-rotating models and may be related to rotational effects. Similar unidentified frequencies are also present in TIC18438742 and TIC385502143, suggesting that rotation may influence the pulsation spectra of these stars. Rotation can alter oscillation frequencies through rotational splitting and structural modifications caused by centrifugal distortion and rotational mixing (S. J. Murphy et al. 2022), while convective core overshooting affects the core size and evolutionary timescale of intermediate-mass stars. Because these effects are not included in the present models, the uncertainties in the derived cluster parameters, particularly the age and metallicity, may be slightly underestimated. Nevertheless, the good agreement between the seismic results and independent constraints from isochrone fitting and spectroscopy indicates that the simplified modeling still provides meaningful constraints on the global properties of the cluster.

7. SUMMARY

In this work, we performed a comprehensive investigation of the open cluster NGC1647 by integrating datasets from space-based missions (*Gaia*, *K2*, and *TESS*) and ground-based facilities (LAMOST, APOGEE, and NOT). From an initial catalog of stars within a 100 pc projected radius of the cluster center, we employed the HDBSCAN algorithm to identify a robust sample of cluster members, adopting a membership probability threshold of $P_{\text{mem}} \geq 0.7$. Subsequent refinement using radial velocities effectively eliminated residual contaminants, resulting in a final sample of 271 high-confidence member stars. The metallicity of NGC1647 was determined to be $[\text{Fe}/\text{H}] = -0.028 \pm 0.021$ dex based on spectroscopic measurements from LAMOST, APOGEE, and R. Carrera et al. (2022). Based on the extinction-corrected magnitudes and color indices of the identified members, traditional isochrone fitting

yields a relatively broad age range, spanning from 125 to 280 Myr.

Leveraging the high-cadence *K2* and *TESS* light curves, we identified 96 periodic variables within the cluster. Among these, nine stars exhibiting p -mode pulsations (comprising five classical δ Sct stars and four hybrid δ Sct- γ Dor stars) provided the basis for our subsequent asteroseismic analysis. We determined the $\Delta\nu$ and identified $\ell = 0$ and $\ell = 1$ pulsation modes using échelle diagram diagnostics. By fitting these seismic constraints against those of a grid of MESA/GYRE evolutionary and pulsation models, we derived a joint asteroseismic solution for the cluster: $\tau = 178_{-9}^{+11}$ Myr and $[\text{Fe}/\text{H}] = -0.08_{-0.01}^{+0.04}$ dex.

This asteroseismic metallicity agrees well with spectroscopic results, while the derived age remains consistent with traditional estimates but offers significantly higher precision. As high-precision time-series photometry continues to grow with future missions like *PLATO* (H. Rauer et al. 2014), the growing census of seismic members will further bolster the robustness of cluster modeling. Such advancements will enable even more stringent constraints on the fundamental parameters of NGC1647 and similar systems, deepening our understanding of stellar and cluster evolution.

ACKNOWLEDGMENTS

We are grateful to the referee for the constructive comments and helpful suggestions, which significantly improved this manuscript. We acknowledge the support from the National Natural Science Foundation of China (NSFC) through the grants 12427804, 12273002, 12503035 and 12541303. This work is supported by the China Manned Space Program with grant no. CMS-CSST-2025-A13, the Tianchi Talent Introduction Plan, and the Central Guidance for Local Science and Technology Development Fund under No. ZYYD2025QY27. M.F. thanks Haozhi Wang, Gang Li, Enrico Corsaro, and Sylvain N. Breton for their valuable and insightful discussions. A.F. acknowledges funding from the Large Grant INAF-2024 “SKYWALKER”.

Facilities: Gaia, Kepler, TESS, LAMOST, APOGEE

Software: HDBSCAN (R. J. G. B. Campello et al. 2013; L. McInnes et al. 2017), Lightkurve (Lightkurve Collaboration et al. 2018), échelle (D. Hey & W. Ball 2020)

REFERENCES

- Aerts, C., Christensen-Dalsgaard, J., & Kurtz, D. W. 2010, *Asteroseismology*, doi: 10.1007/978-1-4020-5803-5
- Arentoft, T., Bouzid, M. Y., Sterken, C., Freyhammer, L. M., & Frandsen, S. 2005, *PASP*, 117, 601, doi: 10.1086/430115

- Arentoft, T., Kjeldsen, H., Nuspl, J., et al. 1998, *A&A*, 338, 909
- Avni, Y. 1976, *ApJ*, 210, 642, doi: [10.1086/154870](https://doi.org/10.1086/154870)
- Bedding, T. R., Murphy, S. J., Hey, D. R., et al. 2020, *Nature*, 581, 147, doi: [10.1038/s41586-020-2226-8](https://doi.org/10.1038/s41586-020-2226-8)
- Bentley, J. L. 1975, *Commun. ACM*, 18, 509–517, doi: [10.1145/361002.361007](https://doi.org/10.1145/361002.361007)
- Berry, I., Huber, D., Li, Y., et al. 2025, arXiv e-prints, arXiv:2510.20048, doi: [10.48550/arXiv.2510.20048](https://doi.org/10.48550/arXiv.2510.20048)
- Borucki, W. J., Koch, D., Basri, G., et al. 2010, *Science*, 327, 977, doi: [10.1126/science.1185402](https://doi.org/10.1126/science.1185402)
- Brogaard, K., Arentoft, T., Miglio, A., et al. 2023, *A&A*, 679, A23, doi: [10.1051/0004-6361/202347330](https://doi.org/10.1051/0004-6361/202347330)
- Buckner, A. S. M., & Froebrich, D. 2014, *MNRAS*, 444, 290, doi: [10.1093/mnras/stu1440](https://doi.org/10.1093/mnras/stu1440)
- Caldwell, D. A., Tenenbaum, P., Twicken, J. D., et al. 2020, *Research Notes of the American Astronomical Society*, 4, 201, doi: [10.3847/2515-5172/abc9b3](https://doi.org/10.3847/2515-5172/abc9b3)
- Campello, R. J. G. B., Moulavi, D., & Sander, J. 2013, in *Advances in Knowledge Discovery and Data Mining*, ed. J. Pei, V. S. Tseng, L. Cao, H. Motoda, & G. Xu (Berlin, Heidelberg: Springer Berlin Heidelberg), 160–172
- Cantat-Gaudin, T., Jordi, C., Vallenari, A., et al. 2018, *A&A*, 618, A93, doi: [10.1051/0004-6361/201833476](https://doi.org/10.1051/0004-6361/201833476)
- Cantat-Gaudin, T., Anders, F., Castro-Ginard, A., et al. 2020, *A&A*, 640, A1, doi: [10.1051/0004-6361/202038192](https://doi.org/10.1051/0004-6361/202038192)
- Carrera, R., Casamiquela, L., Bragaglia, A., et al. 2022, *A&A*, 663, A148, doi: [10.1051/0004-6361/202243151](https://doi.org/10.1051/0004-6361/202243151)
- Chen, Y., Girardi, L., Fu, X., et al. 2019, *A&A*, 632, A105, doi: [10.1051/0004-6361/201936612](https://doi.org/10.1051/0004-6361/201936612)
- Choi, J., Dotter, A., Conroy, C., et al. 2016, *ApJ*, 823, 102, doi: [10.3847/0004-637X/823/2/102](https://doi.org/10.3847/0004-637X/823/2/102)
- Cui, X.-Q., Zhao, Y.-H., Chu, Y.-Q., et al. 2012, *Research in Astronomy and Astrophysics*, 12, 1197, doi: [10.1088/1674-4527/12/9/003](https://doi.org/10.1088/1674-4527/12/9/003)
- Danielski, C., Babusiaux, C., Ruiz-Dern, L., Sartoretti, P., & Arenou, F. 2018, *A&A*, 614, A19, doi: [10.1051/0004-6361/201732327](https://doi.org/10.1051/0004-6361/201732327)
- Dias, W. S., Monteiro, H., Moitinho, A., et al. 2021, *MNRAS*, 504, 356, doi: [10.1093/mnras/stab770](https://doi.org/10.1093/mnras/stab770)
- Dotter, A. 2016, *ApJS*, 222, 8, doi: [10.3847/0067-0049/222/1/8](https://doi.org/10.3847/0067-0049/222/1/8)
- Dupret, M. A., Grigahcène, A., Garrido, R., Gabriel, M., & Scuflaire, R. 2005, *A&A*, 435, 927, doi: [10.1051/0004-6361:20041817](https://doi.org/10.1051/0004-6361:20041817)
- Fritzewski, D. J., Barnes, S. A., Weingrill, J., et al. 2023, *A&A*, 674, A152, doi: [10.1051/0004-6361/202346083](https://doi.org/10.1051/0004-6361/202346083)
- Fu, J.-N., Cat, P. D., Zong, W., et al. 2020, *Research in Astronomy and Astrophysics*, 20, 167, doi: [10.1088/1674-4527/20/10/167](https://doi.org/10.1088/1674-4527/20/10/167)
- Gaia Collaboration, Drimmel, R., Romero-Gómez, M., et al. 2023, *A&A*, 674, A37, doi: [10.1051/0004-6361/202243797](https://doi.org/10.1051/0004-6361/202243797)
- Gautam, A., Murphy, S. J., & Bedding, T. R. 2025, arXiv e-prints, arXiv:2507.03561, doi: [10.48550/arXiv.2507.03561](https://doi.org/10.48550/arXiv.2507.03561)
- Grigahcène, A., Antoci, V., Balona, L., et al. 2010, *ApJL*, 713, L192, doi: [10.1088/2041-8205/713/2/L192](https://doi.org/10.1088/2041-8205/713/2/L192)
- Guerrero, C. A., Peña, J. H., & Sareyan, J. P. 2011, *RMxAA*, 47, 185
- Guzik, J. A., Baran, A. S., Sanjayan, S., et al. 2023, *AJ*, 165, 188, doi: [10.3847/1538-3881/acc0f0](https://doi.org/10.3847/1538-3881/acc0f0)
- Hey, D., & Ball, W. 2020, 1.4 Zenodo, doi: [10.5281/zenodo.3629933](https://doi.org/10.5281/zenodo.3629933)
- Hippke, M., David, T. J., Mulders, G. D., & Heller, R. 2019, *AJ*, 158, 143, doi: [10.3847/1538-3881/ab3984](https://doi.org/10.3847/1538-3881/ab3984)
- Howell, S. B., Sobek, C., Haas, M., et al. 2014, *PASP*, 126, 398, doi: [10.1086/676406](https://doi.org/10.1086/676406)
- Hunt, E. L., & Reffert, S. 2023, *A&A*, 673, A114, doi: [10.1051/0004-6361/202346285](https://doi.org/10.1051/0004-6361/202346285)
- Lada, C. J., & Lada, E. A. 2003, *ARA&A*, 41, 57, doi: [10.1146/annurev.astro.41.011802.094844](https://doi.org/10.1146/annurev.astro.41.011802.094844)
- Li, G., Mombarg, J. S. G., Guo, Z., & Aerts, C. 2025, *A&A*, 703, A116, doi: [10.1051/0004-6361/202556409](https://doi.org/10.1051/0004-6361/202556409)
- Li, G., Van Reeth, T., Bedding, T. R., et al. 2020, *MNRAS*, 491, 3586, doi: [10.1093/mnras/stz2906](https://doi.org/10.1093/mnras/stz2906)
- Lightkurve Collaboration, Cardoso, J. V. d. M., Hedges, C., et al. 2018, *Astrophysics Source Code Library* <http://ascl.net/1812.013>
- Lindegren, L., Klioner, S. A., Hernández, J., et al. 2021, *A&A*, 649, A2, doi: [10.1051/0004-6361/202039709](https://doi.org/10.1051/0004-6361/202039709)
- Liu, C., Fu, J., Shi, J., et al. 2020, arXiv e-prints, arXiv:2005.07210, doi: [10.48550/arXiv.2005.07210](https://doi.org/10.48550/arXiv.2005.07210)
- Liu, L., & Pang, X. 2019, *ApJS*, 245, 32, doi: [10.3847/1538-4365/ab530a](https://doi.org/10.3847/1538-4365/ab530a)
- Lomb, N. R. 1976, *Ap&SS*, 39, 447, doi: [10.1007/BF00648343](https://doi.org/10.1007/BF00648343)
- McInnes, L., Healy, J., & Astels, S. 2017, *The Journal of Open Source Software*, 2, 205, doi: [10.21105/joss.00205](https://doi.org/10.21105/joss.00205)
- McQuillan, A., Mazeh, T., & Aigrain, S. 2014, *ApJS*, 211, 24, doi: [10.1088/0067-0049/211/2/24](https://doi.org/10.1088/0067-0049/211/2/24)
- Mowlavi, N., Holl, B., Lecoœur-Taïbi, I., et al. 2023, *A&A*, 674, A16, doi: [10.1051/0004-6361/202245330](https://doi.org/10.1051/0004-6361/202245330)
- Moździerski, D., Pigulski, A., Kolaczowski, Z., et al. 2019, *A&A*, 632, A95, doi: [10.1051/0004-6361/201936418](https://doi.org/10.1051/0004-6361/201936418)
- Murphy, S. J., Bedding, T. R., White, T. R., et al. 2022, *MNRAS*, 511, 5718, doi: [10.1093/mnras/stac240](https://doi.org/10.1093/mnras/stac240)
- Murphy, S. J., Hey, D., Van Reeth, T., & Bedding, T. R. 2019, *MNRAS*, 485, 2380, doi: [10.1093/mnras/stz590](https://doi.org/10.1093/mnras/stz590)
- Murphy, S. J., Shibahashi, H., & Kurtz, D. W. 2013, *MNRAS*, 430, 2986, doi: [10.1093/mnras/stt105](https://doi.org/10.1093/mnras/stt105)

- Palakkatharappil, D. B., & Creevey, O. L. 2023, *A&A*, 674, A146, doi: [10.1051/0004-6361/202243624](https://doi.org/10.1051/0004-6361/202243624)
- Pamos Ortega, D., García Hernández, A., Suárez, J. C., et al. 2022, *MNRAS*, 513, 374, doi: [10.1093/mnras/stac864](https://doi.org/10.1093/mnras/stac864)
- Pamos Ortega, D., Mirouh, G. M., García Hernández, A., Suárez Yanes, J. C., & Barceló Forteza, S. 2023, *A&A*, 675, A167, doi: [10.1051/0004-6361/202346323](https://doi.org/10.1051/0004-6361/202346323)
- Panda, S. K., Dhanpal, S., Murphy, S. J., Hanasoge, S., & Bedding, T. R. 2024, *ApJ*, 960, 94, doi: [10.3847/1538-4357/ad0a97](https://doi.org/10.3847/1538-4357/ad0a97)
- Paxton, B., Bildsten, L., Dotter, A., et al. 2011, *ApJS*, 192, 3, doi: [10.1088/0067-0049/192/1/3](https://doi.org/10.1088/0067-0049/192/1/3)
- Paxton, B., Cantiello, M., Arras, P., et al. 2013, *ApJS*, 208, 4, doi: [10.1088/0067-0049/208/1/4](https://doi.org/10.1088/0067-0049/208/1/4)
- Paxton, B., Marchant, P., Schwab, J., et al. 2015, *ApJS*, 220, 15, doi: [10.1088/0067-0049/220/1/15](https://doi.org/10.1088/0067-0049/220/1/15)
- Paxton, B., Schwab, J., Bauer, E. B., et al. 2018, *ApJS*, 234, 34, doi: [10.3847/1538-4365/aaa5a8](https://doi.org/10.3847/1538-4365/aaa5a8)
- Paxton, B., Smolec, R., Schwab, J., et al. 2019, *ApJS*, 243, 10, doi: [10.3847/1538-4365/ab2241](https://doi.org/10.3847/1538-4365/ab2241)
- Qin, M., Fu, J.-N., Zong, W., et al. 2025, *ApJS*, 280, 19, doi: [10.3847/1538-4365/adfla9](https://doi.org/10.3847/1538-4365/adfla9)
- Rauer, H., Catala, C., Aerts, C., et al. 2014, *Experimental Astronomy*, 38, 249, doi: [10.1007/s10686-014-9383-4](https://doi.org/10.1007/s10686-014-9383-4)
- Riello, M., De Angeli, F., Evans, D. W., et al. 2021, *A&A*, 649, A3, doi: [10.1051/0004-6361/202039587](https://doi.org/10.1051/0004-6361/202039587)
- Ruíz Díaz, M. A., Aidelman, Y. J., Baume, G., & Granada, A. 2025, *MNRAS*, 537, 1763, doi: [10.1093/mnras/staf114](https://doi.org/10.1093/mnras/staf114)
- Scargle, J. D. 1982, *ApJ*, 263, 835, doi: [10.1086/160554](https://doi.org/10.1086/160554)
- SDSS Collaboration, Adamane Pallathadka, G., Aghakhanloo, M., et al. 2025, arXiv e-prints, arXiv:2507.07093, doi: [10.48550/arXiv.2507.07093](https://doi.org/10.48550/arXiv.2507.07093)
- Stello, D., Basu, S., Bruntt, H., et al. 2010, *ApJL*, 713, L182, doi: [10.1088/2041-8205/713/2/L182](https://doi.org/10.1088/2041-8205/713/2/L182)
- STScI. 2016, STScI/MAST, doi: [10.17909/T9WS3R](https://doi.org/10.17909/T9WS3R)
- Sun, M., Townsend, R. H. D., & Guo, Z. 2023, *ApJ*, 945, 43, doi: [10.3847/1538-4357/acb33a](https://doi.org/10.3847/1538-4357/acb33a)
- Tarricq, Y., Soubiran, C., Casamiquela, L., et al. 2022, *A&A*, 659, A59, doi: [10.1051/0004-6361/202142186](https://doi.org/10.1051/0004-6361/202142186)
- TESS Team. 2021, STScI/MAST, doi: [10.17909/T9-NMC8-F686](https://doi.org/10.17909/T9-NMC8-F686)
- Townsend, R. H. D., Goldstein, J., & Zweibel, E. G. 2018, *MNRAS*, 475, 879, doi: [10.1093/mnras/stx3142](https://doi.org/10.1093/mnras/stx3142)
- Townsend, R. H. D., & Teitler, S. A. 2013, *MNRAS*, 435, 3406, doi: [10.1093/mnras/stt1533](https://doi.org/10.1093/mnras/stt1533)
- Van Reeth, T., Tkachenko, A., Aerts, C., et al. 2015, *A&A*, 574, A17, doi: [10.1051/0004-6361/201424585](https://doi.org/10.1051/0004-6361/201424585)
- Waelkens, C. 1991, *A&A*, 246, 453
- Wang, X., Zong, W., Ma, X.-Y., et al. 2025, *A&A*, 693, A63, doi: [10.1051/0004-6361/202452309](https://doi.org/10.1051/0004-6361/202452309)
- Xing, K., Zong, W., Silvotti, R., et al. 2024, *ApJS*, 271, 57, doi: [10.3847/1538-4365/ad2ddd](https://doi.org/10.3847/1538-4365/ad2ddd)
- Yakut, K., Kalomeni, B., Rappaport, S., & Kostov, V. 2025, *MNRAS*, doi: [10.1093/mnras/staf1731](https://doi.org/10.1093/mnras/staf1731)
- Zdaniavičius, J., Straižys, V., Chen, C. W., et al. 2005, *Baltic Astronomy*, 14, 179
- Zhao, G., Zhao, Y.-H., Chu, Y.-Q., Jing, Y.-P., & Deng, L.-C. 2012, *Research in Astronomy and Astrophysics*, 12, 723, doi: [10.1088/1674-4527/12/7/002](https://doi.org/10.1088/1674-4527/12/7/002)
- Zong, W., Fu, J.-N., De Cat, P., et al. 2020, *ApJS*, 251, 15, doi: [10.3847/1538-4365/abbb2d](https://doi.org/10.3847/1538-4365/abbb2d)